Simulation, experimental validation and kinematic optimization of a Stirling engine using air and helium

Juliette Bert, Daniela Chrenko, Tonino Sophy, Frédéric Sirot, Luis Le Moyne

Simulation, experimental validation and kinematic optimization of a Stirling engine using air and helium

Juliette Bert [a, b], Daniela Chrenko [a, *], Tonino Sophy [a], Luis Le Moyne [a], Frédéric Sirot [b]

[a] DRIVE ID-MOTION, EA 1859 ISAT, U. Bourgogne, 49 rue Mlle Bourgeois, 58000 Nevers, France
[b] Danielson Engineering, Technopôle, 58470 Magny-Cours, France

A Stirling engine with nominal output power of 1 kW is tested using air and helium as working gases. The influence of working pressure, engine speed and temperature of the hot source is studied, analyzing instantaneous gas pressure as well as instantaneous and stationary temperature at different positions to derive the effective power. A zero dimensional finite-time thermodynamic, three zones model of a generic Stirling engine is developed and successfully validated against experimental gas temperature and pressure in each zone, providing the effective power. This validation underlines the interest of different working gases as well as different geometric configurations for different applications. Furthermore, the validated model allows parametric studies of the engine, with regard to geometry, working gas and engine kinematics. It is used in order to optimize the kinematic of a Stirling engine for different working points and gases.

1. Introduction

The need of cheap and clean energy is constantly increasing [1]. At the moment, the most used types of energy conversion machines are: piston type internal combustion engines, gas turbines and steam turbines. Due to their thermodynamic processes, they release hot gases and require cooling, both imposing heat losses. One solution to revalue these losses is the use of external heat engines [2]. As Stirling engines draw their primary energy from externally produced heat, they can be driven by all kinds of heat sources, like exhaust gases, combustion processes using petroleum fuels, combustible gases or vegetable waste and even natural heat energy like solar and geothermal [3–6].

Stirling engines were invented in 1816 by Robert Striling [7] and industrialized shortly after, but most of them were replaced by internal combustion engines in the early 20th century. From the 1930s Phillips starts important research activities on Stirling engines. First, they were meant to power radio stations, but the invention of semiconductor devices put an end to this development. The recent scientific progress in thermal and fluid sciences as well as new materials allowed the creation of sophisticated Stirling engines and the study of different working gases [8]. Stirling engines are nowadays used industrially for cryogenic [9] portable and mobile applications [10], since the 1980s Stirling engines are also studied in combination with solar energy [4,11]. The need of more efficient engines for mobile as well as stationary applications explains the regained interest in Stirling engines.

Since the invention of the Stirling engine, its modeling – a complex problem including mass flow, thermal flow and thermodynamic evolution – has been studied by different researchers starting with the first model by Schmidt in 1871 [12–29]. For isothermal modeling the motor is split into three zones (cold, hot and regenerator) and the gas temperature in each zone is considered as constant. Several developments are made based on this first simple isothermal model. These improvements include the impact of the regenerator efficiency by Kongtragool and Wongwises [16] as well as Ahmadi et al. [23], whereas Puech and Tishkova [17] studied the impact of the dead volume for different kinematics. Blank [13], Costea and Feidt [14], Kaushik and Kumar [15], Wouagfack and Tchinda [24] as well as Kantor an Mousaw [25] modeled the heat source as finite elements. Ladas [26] as well as Ahmadi et al. [21] used finite time approach to describe a solar-powered Striling engine. To overcome the drawbacks of homogeneous temperature zones Urieli and Berchowitz [20] developed a model considering the compression and expansion of the volume as adiabatic and integrated imperfect exchangers. Costa et al. [27] proposed an analytical approach to describe the regenerator pressure loss.

* Corresponding author. Tel.: +33 3 86 71 50 66.
E-mail addresses: daniela.chrenko@u-bourgogne.fr (D. Chrenko), tonino.sophy@u-bourgogne.fr (T. Sophy), luis.le-moyne@u-bourgogne.fr (L. Le Moyne).

Nomenclature

h	specific enthalpy, J/kg
k	convection coefficient, W/(m^2.K)
m	mass, kg
p	pressure, Pa
Q	heat, J
r	specific gas constant, J/(kg/K)
S	flow section between two consecutive zones, m^2
T	temperature, K
u	specific internal energy, J/kg
V	volume, m^3
v	particles speed
x	particles position
xg	best position reached by all the swarm
xp	best position reached by one particle

Subscripts

c	cold zone
cr, c_r	between cold zone and regenerator
h	hot zone
hr, h_r	between hot zone and regenerator
m	regenerator matrix
r	regenerator zone
w	wall

Hence, even if the temperature in each zone is uniform, it evolves during a cycle. Abbas et al. [12] and Timoumi et al. [19,28] concentrate on this approach whilst adding different losses (conduction and pressure drop). Özgören et al. [29] present an artificial neural network based model of a beta-type Stirling engine using helium as working gas.

Recently a special interest is put on the optimization of Stirling engines in order to achieve optimum power and efficiency levels [30–32]. Multi-objective optimization of power and efficiency was conducted by Ahmadi et al. [4,21–23]. Chen and Yang [30] used a thermodynamic model in order to optimize geometric parameters, Creyx et al. [31] optimize the pressure and temperature range and a combined approach is presented by Campos et al. [32].

Here, a zero dimensional 3 zones model is developed. In this model, time dependent heat transfers are considered in each zone. One of the purposes of the model is to allow parametric studies of system parameters and kinematics for different working gases, over a wide range of filling pressures and hot side temperatures. Therefore it has to be simple enough to test different sets of parameters and at the same time provide accurate results.

This study consists of four sections. First, the experimental rig of a 1 kW gamma type Stirling engine that has been adapted to our needs is presented. The influence of the variation of the following parameters is studied: working gas (air and helium), gas pressure, hot zone temperature as well as engine speed. For all experiments, evolution of temperature and pressure inside the working zones is measured in order to evaluate the indicated power. Torque and speed are measured in order to evaluate the effective power. Secondly, a three zone zero dimensional finite-time thermodynamic model is developed. After a short description of the proposed model, numerical and experimental results for different parameters are compared. Eventually, a tool to assist Stirling engine design is developed using the model, to which an optimization algorithm is added. This tool allows to sketch out a preliminary draft of the characteristics of a Stirling engine during the first step of the design study. Depending on the desired application and on the constraints exerted on the engine, the tool will act on the characteristics of the engine chosen by the user (e.g. dimensions, kinematics) to maximize its performance.

2. Experimental rig

2.1. Engine description

Based on the ST05G-CNC Stirling engine [33], an experimental rig is developed to evaluate the impact of some experimental conditions and geometrical characteristics of Stirling engine. Two different working gases are tested: air and helium. Helium is considered as interesting alternative working gas, due to the difference in gas behavior, namely density and heat capacity [3,34].

2.1.1. Engine characteristics

As the tested engine is a gamma type Stirling engine (Figs. 1 and 2) the internal gas flow is defined by a pair of pistons. The first, or power piston, transforms thermodynamic energy in physical displacement and therefore work. The second, or displacer piston, has to displace the gas from cold zone to hot zone and inversely across the regenerator. The two pistons are connected to the same crankshaft with a phase difference of 90°. Their stroke is 75 mm, the power piston's bore is 85 mm and the displacer piston's is 96 mm. The total internal volume of the engine when the power piston is at the bottom dead center is 1.9 dm^3.

On the cold side, water circulation around cylinder and exchanger maintains the temperature, thus defining the cold temperature of the cycle. On the hot side, there are heating resistances which bring heat energy to the engine across cylinder wall and tight tubes. The regenerator is made of a stainless steel matrix grid.

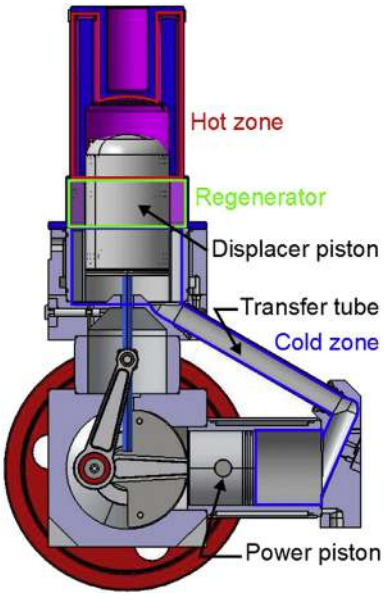

Fig. 1. Section view of the tested engine.

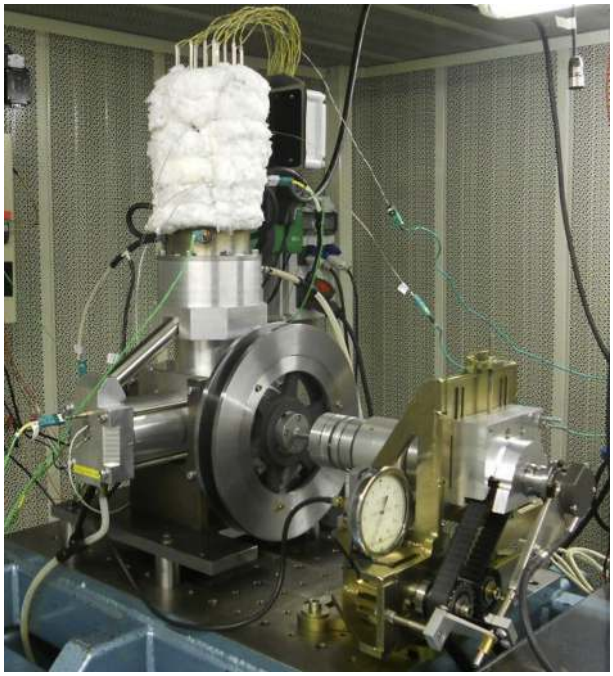

Fig. 2. Stirling engine on test rig.

2.1.2. Instrumentation

Sensors are devoted to measure the thermodynamic state of gas in each of the three zones. Three instantaneous piezo resistive pressure sensors are installed. They have a pressure range between 0 and 13.5 bar relative, a precision of 80 mbar and an acquisition frequency of 200 kHz. Furthermore, three K-type micro-thermocouples with a diameter of 25 μm are used at a frequency of 10 kHz. Their values are linearized over the temperature range.

The external state of the engine is measured using five K-type thermocouples (one on the cold side and four on the hot side) with wire diameter of 1 mm, which are introduced into the walls of cold and hot sides to evaluate a representative value of the mean exchange temperature between walls and gas.

Finally, as an electrical cartridge based hot source is used, the power needed to maintain the hot wall temperature during engine run is measured. Furthermore, the output torque of the engine is measured using a torquemeter with a rated torque of −50+50 Nm, a precision of 0.25 Nm and a resolution of 60 pulses per revolution as well as a speed measurement using a 0.5° precision encoder in order to calculate its effective power.

2.2. Test conditions

The experimental rig allows to evaluate the impact of various parameters on engine behavior. Four parameters were selected for analysis: three operating conditions (speed, hot side temperature and filling pressure) and one working gases condition: air or helium.

An electrical engine is connected to the Stirling engine drive shaft to control its speed. With the control of a variator and a brake resistance it is possible to regulate the speed of the engine in a range from 200 rpm to 1000 rpm.

The electrical power supply of the heating resistances is controlled according to the value of the temperature measured by a thermocouple on the hot site. The maximum power of the heating resistances is 7 kW and allows to test this engine for hot side temperatures up to 700 °C. The temperature of the cold sink is maintained with circulation of industrial aero-cooled water at around 25 °C.

As the tests are carried out with different filling pressures, a particular attention is devoted to track potential leaks. To counteract gas leaks, the system was kept under pressure by an external device. Nevertheless, a comparison between plugged engine pressure curves and unplugged engine ones has been made. It shows that the external pressurized gas supply does not significantly change results. Pressure values ranking from 1 bar relative to 10 bar relative are used.

The results section presents values that do not vary over a cycle like hot and cold source temperature or filling pressure, and instantaneous values, that vary over a cycle, like cylinder volume and pressure. For all instantaneous parameters, averaged values over 100 cycles are presented in order to minimize the influence of measurement errors.

3. Model

3.1. Goal of the model

The main objective of the model is to have a tool that is able to provide predictive trends of engine performance. Hence an emphasis must be put on the modularity in order to making the model be able to optimize the characteristics of an engine corresponding to constraints like power and weight. A more detailed description of the model by Bert et al. can be found in Ref. [35].

The first particularity of this model compared to Abbas et al. [12], Kongtragool and Wongwises [16], and Andersen et al. [36], is the use of time-dependent non isothermal exchangers. This means that the equations introduced in the next section are instantaneous and solved for each time step. This introduces the evolution of certain parameters like the temperatures and pressures of the gas inside the pistons as well as the regenerator temperature. At the same time, thermal inertia imposes that other parameters like the wall temperature of the hot and cold source stay constant throughout the cycle.

Moreover, a three zones model is created, describing the wall surface and temperature for each zone in function of the geometry (cylinder, exchanger …). The regenerator is described as a heat exchanger between its matrix and the gas. Thus, the model takes into account its ability to store and release a part of the heat intrinsically as in Ref. [4] and the use of an arbitrary efficiency coefficient, like in Ref. [28], is not needed anymore. Each of the three zones corresponds to a volume exchanging heat with a hot source (zone 1), a cold source (zone 3), and a regenerator (zone 2). Heat exchanges, heat losses as well as leaks can be affected to all three zones. A working gas describes a cycle determined by a given (but not fixed) kinematic of pistons or moving surfaces transferring gases from one zone to another. Gases are considered as ideal [37] and thermodynamic variables are considered homogeneous in each volume, (Fig. 3).

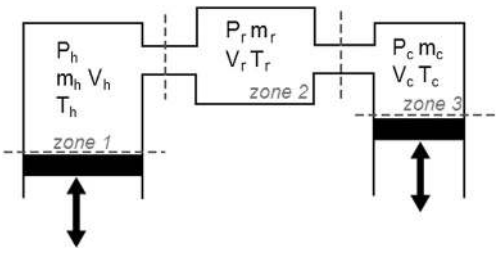

Fig. 3. Various zones of the model.

3.2. Model description

Hot volume V_h and cold volume V_c are defined by piston displacements, which depend on the crank angle and can thus be calculated geometrically. The regenerator volume V_r is constant. There are thus three unknowns in each zone; the pressures p_h, p_c, p_r, the masses m_h, m_c, m_r and the gas temperatures T_h, T_c, T_r. Moreover, the temperature of the regenerator matrix T_m has to be considered as additional unknown as it evolves throughout the cycle due to the exchange with the gases which pass through. A differential equation system with 10 unknowns is thus developed based on the perfect gas law, Eqs. (1), (4), (7), the energy conservation due to the second law of thermodynamics, Eqs. (2), (5), (8), and the mass conservation, Eqs. (3), (6), (9), for the cold, hot and regenerator zone respectively, and energy conservation Eq. (10) for the regenerator matrix.

Cold volume (c)

$$m_c \cdot r \cdot \mathrm{d}T_c + r \cdot T_c \cdot \mathrm{d}m_c - V_c \cdot \mathrm{d}p_c = p_c \cdot \mathrm{d}V_c \tag{1}$$

$$u_c \cdot \mathrm{d}m_c + m_c \cdot \mathrm{d}u_c - h_{cr}\mathrm{d}m_c = -p_c \cdot \mathrm{d}V_c + \delta Q_c \tag{2}$$

$$\mathrm{d}m_c = \mathrm{flow}_{c_r} \tag{3}$$

Hot volume (h)

$$m_h \cdot r \cdot \mathrm{d}T_h + r \cdot T_h \cdot \mathrm{d}m_h - V_h \cdot \mathrm{d}p_h = p_h \cdot \mathrm{d}V_h \tag{4}$$

$$u_h \cdot \mathrm{d}m_h + m_h \cdot \mathrm{d}u_h - h_{hr}\mathrm{d}m_h = -p_h \cdot \mathrm{d}V_h + \delta Q_h \tag{5}$$

$$\mathrm{d}m_h = \mathrm{flow}_{h_r} \tag{6}$$

Regenerator (r)

$$m_r \cdot r \cdot \mathrm{d}T_r + r \cdot T_r \cdot \mathrm{d}m_r - V_r \cdot \mathrm{d}p_r = p_r \cdot \mathrm{d}V_r \tag{7}$$

$$u_r \cdot \mathrm{d}m_r + m_r \cdot \mathrm{d}u_r + h_{cr} \cdot \mathrm{d}m_c + h_{hr}\mathrm{d}m_h = \delta Q_r \tag{8}$$

$$\mathrm{d}m_h = -\mathrm{d}m_c - \mathrm{d}m_h - \mathrm{d}m_{\mathrm{leackage}} \tag{9}$$

$$m_m \cdot \mathrm{d}u_m = \delta Q_m \tag{10}$$

where r is the specific gas constant, u is the specific internal energy and δQ is the heat difference.

This system is solved numerically with Matlab using a variable order solver based on the numerical differentiation equations [38,39] with an absolute convergence criterion of 10^{-6}. Initial conditions are defined for the 10 unknowns which allow a cold or a hot start.

Different values used in the main equations have been calculated in subfunctions and can be modified independently.

The position and velocity of each piston can be calculated using the mechanical link and some geometrical dimensions influencing the volume as for example the length of rod, stroke or phase difference. Therefore, the cylinder volumes as well as the dead volume are known at each moment.

Thermal exchanges between gas and surface describe the energy supply to or from the motor. This mainly convective energy exchange is described using the Newton law [40], depending on exchange surface, temperature difference between the surface and the gas and the convective exchange coefficient.

$$\mathrm{d}Q = k \cdot S \cdot \left(T_{\mathrm{surface}} - T_{\mathrm{gas}}\right) \tag{11}$$

The exchange coefficients k depend on motor speed as well as gas temperature and pressure, and are obtained using Colburn correlation [35]. The thermal inertia of the components is supposed to be big enough to assume a constant temperature of the walls during the cycle.

Frequently, convective heat transfer inside cylinders are described by a correlation of the Nusselt number obtained by experiments. Seghir-Ouali et al. [41] use inverse or analytic methods to determine coefficients of the Nusselt correlation of an inside rotating cylinder flow. Their paper also presents a considerable literature review.

Inner instationary cylinder flow heat transfers are often characterized using the Colburn correlation [42], even though this correlation was developed for established flows. Only few cases studying alternative direction fluid flows are known, which means that a model improvement might be reached using an correction factor.

A mass exchange occurs between cold zone and regenerator as well as between hot zone and regenerator. Exchanges between working gas and vicinity could also be calculated in order to describe potential leakage. In order to describe the mass flow between two zones based on a given geometry, the pressure difference on both sides is evaluated by the Saint−Venant equation [43,44]. Even thought it is generally used to describe the condition as at inlet/outlet of internal combustion engines [45], it can be applied here to calculate the mass flow. Furthermore, pressure loss due to the obstacle is considered.

$$\mathrm{d}m = S_i \frac{P_j}{\sqrt{r \times T_j}} \left(\frac{P_i}{P_j}\right)^{1/\gamma} \sqrt{\frac{2\gamma}{\gamma - 1}\left(1 - \left(\frac{P_i}{P_j}\right)^{\frac{\gamma-1}{\gamma}}\right)} \tag{12}$$

To reinforce this approach, pressure drops have been tested for the three zones of the Stirling engine with air as working gas using an internal wind tunnel. The results allowed to derive equations of pressure drop in function of air speed for each zone. Those results have also been applied for helium as working gas, as it was not possible to do the tests using helium with the available means. An analytical approach to describe the regenerator pressure loss has been described by Costa et al. [27], but it considers only air as working gas.

The thermodynamic characteristics of the gases have been calculated using Janaf tables [46] or equivalent approaches. The characteristics of gas (heat capacity, Reynolds number, etc.) are determined by which working gas is used.

4. Results and discussion

4.1. Influence of speed

Fig. 4 presents the thermodynamic cycle on the cold and hot side using air and helium as working gases for the extreme speeds 200 rpm and 1000 rpm. The experimental results are well in line with modeling results. It is interesting to observe that for air as working gas, the variation of the PV diagram between 200 rpm and 1000 rpm is small both for hot and cold side.

Regarding the results for helium as working gas, it can be seen that the modeling results show no variation with rotational speed. Experimental results show a bigger pressure variation for 1000 rpm than for 200 rpm, both for hot and cold side. This implies furthermore that the effected work is higher at faster rotational speed. This can be explained by the fact that at 200 rpm the exchange time is relatively long and the heat storage is limited by the relative small value of ρC_p of helium. At faster rotational speed the exchange time

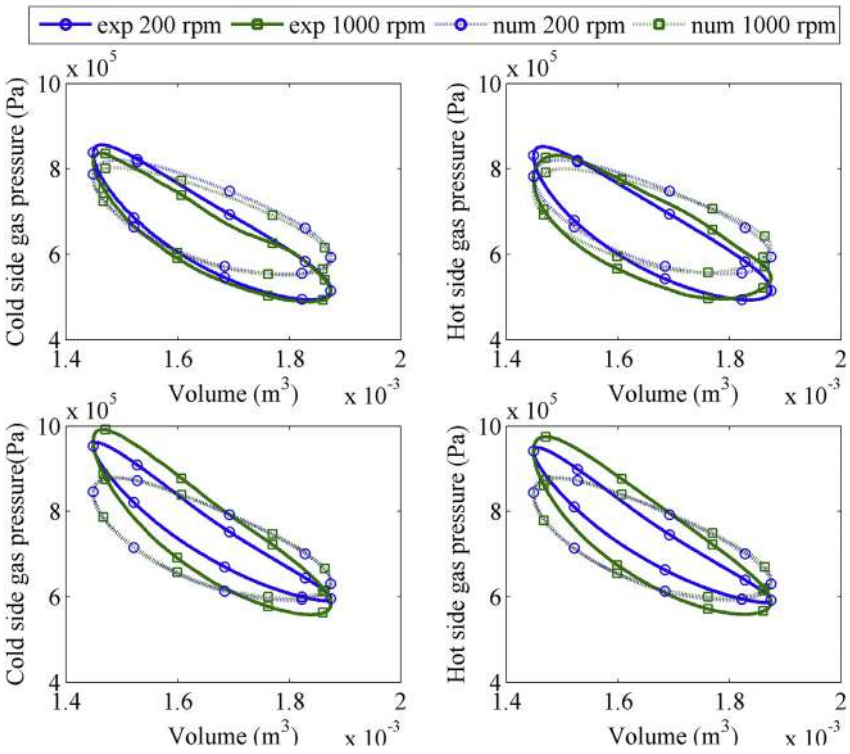

Fig. 4. PV diagram of speed influence on gas pressure - air [top] and helium [bottom] (Twh = 700 °C, P_{mot} = 7 bar, tube 1).

is much shorter and the amount of heat to be stored is smaller. Hence the limited heat storage capacity is less penalizing.

The numerical results vary little for the tested speeds. This can be explained by the fact that the pressure drop for helium has been adapted from the values measured for air (see Section 3.2). This underlines the necessity to put an emphasis on the influence of pressure drop in function of gas characteristics in further works. However, the tendencies obtained by the variation of the respective parameters are taken into account correctly and the results obtained from optimization (see Section 5.2) will give the correct tendencies.

Finally, in Fig. 5 we can observe the influence of engine speed on effective power for different temperatures for both gases. The influence of the rotational speed on the power is described in the same way by experimental and numerical results. Furthermore, it can be seen that for air as working gas an optimal rotational speed in order to maximize the power delivered exists, the numerical model is able to predict the optimal rotational speed for different temperatures with good accuracy. The maximum power that can be attained, increases with increasing hot side temperature. Moreover, the maximum power occurs at higher rotational speeds if the hot side temperature increases.

However, for helium as working gas, numerical and experimental results predict that the maximum power is not reached in the range of rotational speeds given by the experimental installation. It can be predicted that the maximum power that can be reached using helium as working gas will be at higher values and higher rotational speeds compared to air. Moreover, at low rotational speed air shows better indicated powers than helium no matter the temperature.

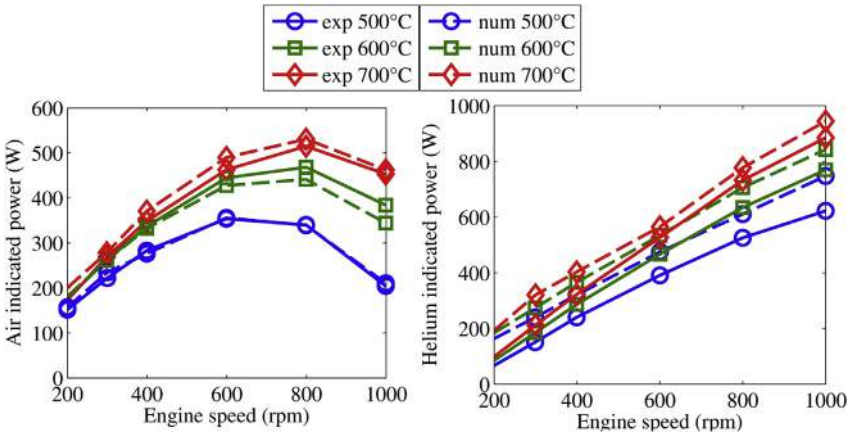

Fig. 5. Effective power in function of speed for various hot side temperature (P_{mot} = 7 bar, tube 1).

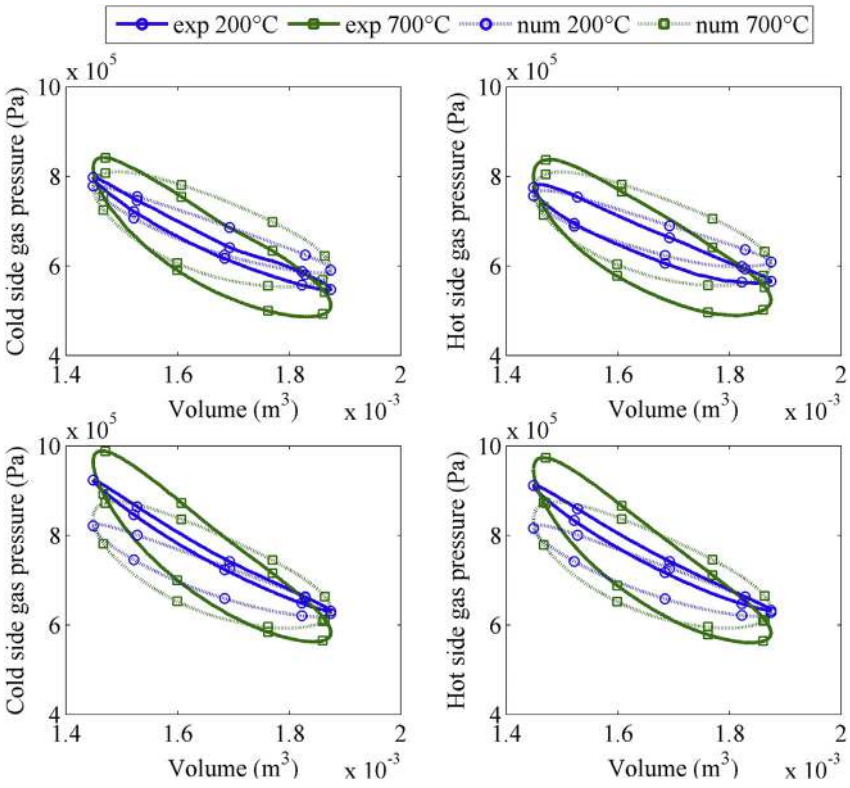

Fig. 6. PV diagram of hot side temperature influence – air [top] and helium [bottom] ($N = 600$ rpm, $P_{mot} = 7$ bar, tube 1).

Air has a better heat storage capacity but a lower heat conductivity coefficient than helium. This explains that for low speed, when the gases have time to exchange with the wall, air has the capacity to store more energy than helium, but when the speed increases, the air has not enough time to store as much heat as in low speed. Moreover, helium benefits from its convective exchange coefficient – which increases with engine speed – to incorporate heat faster. This, added to the lower density of helium compared with the air's, explains the differences in power variation. This phenomenon has also been described by Karabulut et al. [8,47].

4.2. Influence of hot side temperature

Fig. 6 shows the influence of the hot side temperature on the PV diagram, using 200°C and 700°C. For both working gases, an increase of hot side temperature leads to an increase of the amplitude of pressure and thus an increase in terms of performance.

The coherence between experimental and numerical results is acceptable for both air and helium, however the reason for the slightly greater differences for helium has already been indicated above (Section 4.1).

As the hot side temperature has an impact on the instantaneous gas pressure without distinction of gas, it is without surprise that Fig. 7 shows the effective power increases in the same way for both gases, and this for all speeds. Furthermore, the different slopes of the curves underline the observation that the optimal rotational speed increases with the temperature.

This evolution is described with a good precision by the model in the case of air as working gas. Despite of the slight

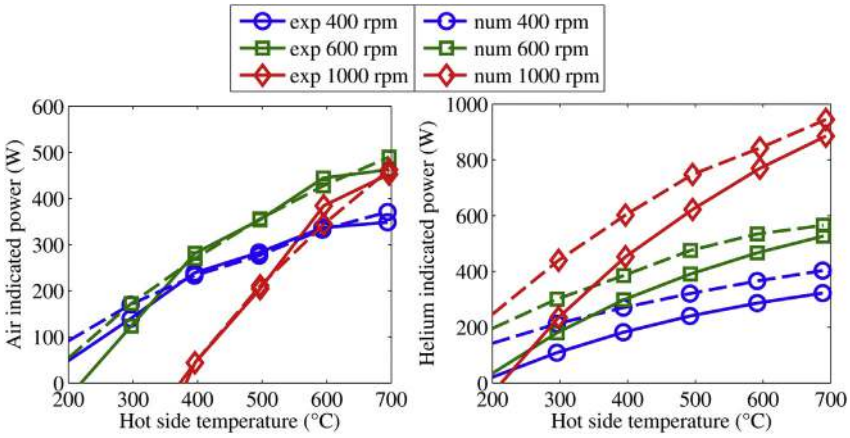

Fig. 7. Effective power in function of hot side temperature for various speed ($P_{mot} = 7$ bar, tube 1).

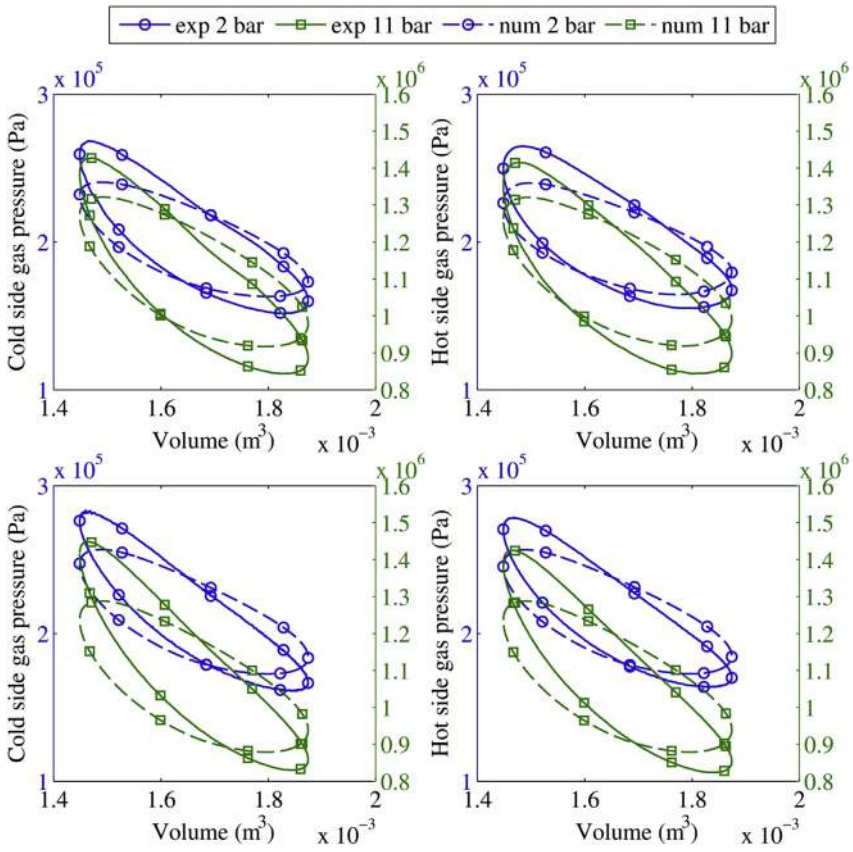

Fig. 8. Filling pressure influence on instantaneous gas pressure – air [top] and helium [bottom] (N = 600 rpm, Twh = 700 °C, tube 1).

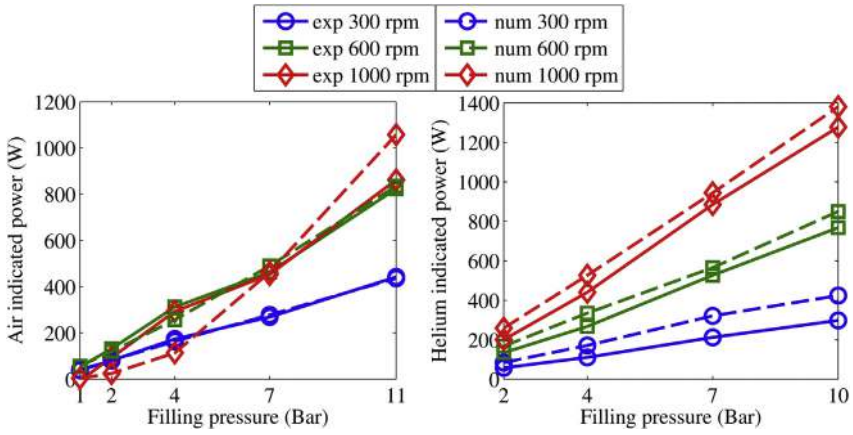

Fig. 9. Effective power in function of filling pressure for various speed (Twh = 700 °C, tube 1).

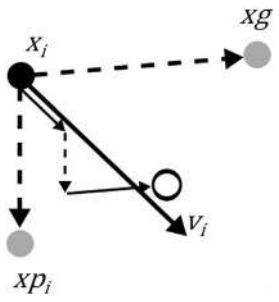

Fig. 10. Scheme of particle displacement.

overestimation of power by the numerical model for helium due to the reasons described in Section 4.1, the tendency of power evolution as function of temperature for different rotational speeds is described correctly.

Table 1
Dimension of the motor in mm.

	Bore	Stroke	Rod
Piston	85	75	146
Displacer	96	75	130

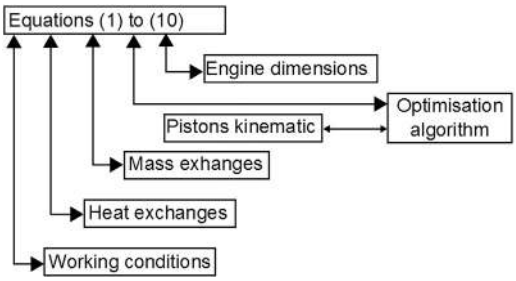

Fig. 11. Association of model to PSO for power maximization in function of kinematics.

4.3. Influence of filling pressure

Fig. 8 shows the PV diagram of hot and cold side for air and helium with filling pressure of 2 bar absolute and 11 bar absolute. As expected the filling pressure of the Stirling engine has a strong influence on the mean value of the pressure during a cycle. The pressure drop depends mainly on the two gas characteristics, density and viscosity, and both are influenced by pressure. No matter which gas is used, density increases with pressure, and leads to an increased pressure drop. Viscosity decreases when pressure increases, and leads to a decreased pressure drop. Although, as the increment of density is faster for air than for helium and the decrease of viscosity is slower for air than helium, an increase of filling pressure leads to a relative reduction of helium pressure drop compared to air pressure drop. This explains why the engine is more efficient using helium at high pressures.

The numerical results show acceptable accuracy for the range of filling pressures. However, it can be observed that the model based value of pressure variation is less than the measured value and this phenomenon is slightly bigger for helium due to the reasons introduced above.

As has been predicted using the PV diagrams in Fig. 8, it can be seen in Fig. 9 that effective power increases with the filling pressure no matter which working gas is used. This phenomenon is described correctly by the simulation.

5. Optimization

After a model validation over a large range of temperatures, pressures and rotational speeds, it can be used to predict the influence of certain parameters like dimensions and kinematics on the performance of a Stirling engine. Depending on the application for which the Stirling engine is foreseen, different constraints have to be applied. For example, a stationary application will have less constraints on the weight of the system than a mobile application. The heat source will also have a considerable influence depending on its availability.

This is why the model presented in Section 3 is associated to an optimization algorithm that permits to find a first approach of an optimized Stirling engine for a given application.

5.1. Particle swarm optimization

In order to achieve the optimization of the model, a multivariable optimization algorithm is needed. The algorithms that are best adapted for this case are stochastic methods that use aleatory parameters and avoid local optima. Different algorithms like genetic algorithms, based on evolution, or biologic algorithms, based on group behavior, may lead to a solution [48]. Özgören et al. [29] used an artificial neural network based approach in order to describe a beta-type Stirling engine, Ahmadi et al. [3,4,22,23] did multi-objective optimization with regard to efficiency and power density using an evolutionary algorithm.

Finally, PSO (particle swarm optimization) was chosen for our case, due to its facility of use and quick convergence. This algorithm was developed in 1995 by Russell Eberhard and James Kennedy [49]. The working principle of PSO is based on a postulate that the communication between individuals of a group allows this group to act more intelligently than the sum of all individual intelligence, for example in a swarm of bees.

A domain with j dimensions is defined. The dimensions correspond to the number of parameters that have to be optimized and their limits are defined by the problem. At initialization a number of i individuals is defined randomly and their objective function value is evaluated. Each individual has a memory of its own best position and the global best position of the group is exchanged by communication. For the next step, every particle moves due to three influences. Firstly, every particle follows its inertia, which pushes it to follow its path. Secondly, their experience pushes a particle to return to its known historical best position. Thirdly, it tends to follow group instinct and to go to the global best position of the group. Finally, a random factor can be added to balance the three influences. A superposition of those three instincts gives the new position of the particle, (Fig. 10). This behavior continues until a satisfaction criterion is reached.

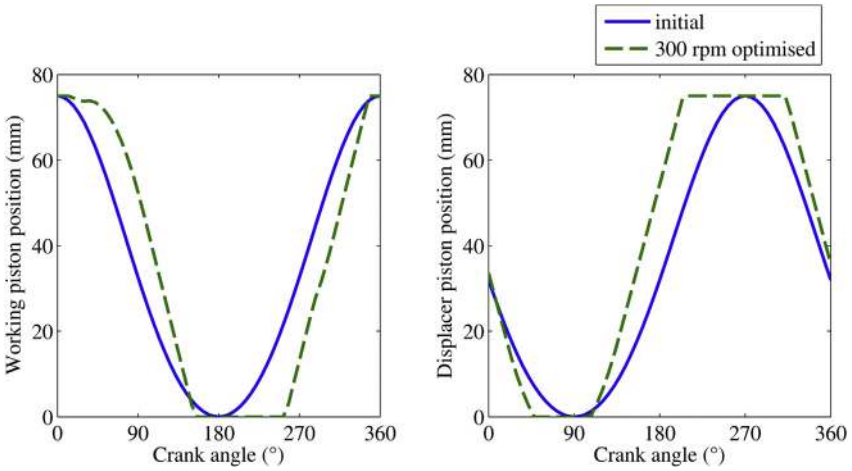

Fig. 12. Optimized piston kinematics: air, 10 bar, 300 rpm, 700 °C.

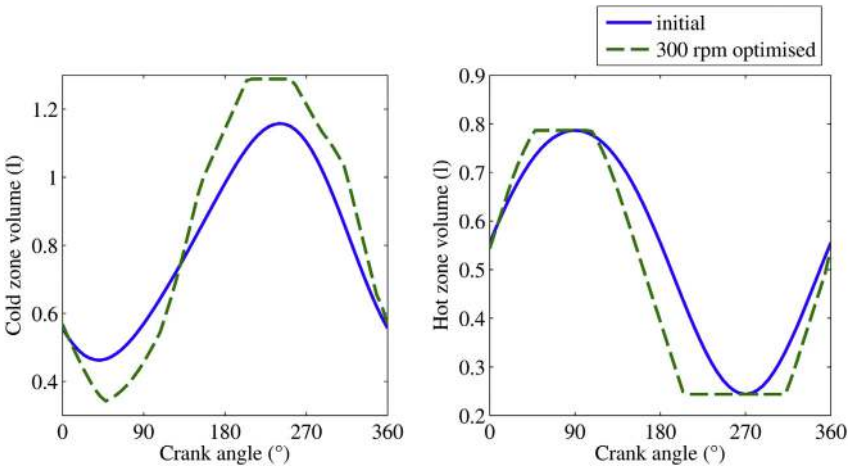

Fig. 13. Optimized volumes: air, 10 bar, 300 rpm, 700 °C.

5.2. Optimization of kinematics

The optimization introduced before is used in order to optimize the kinematics of a Stirling engine with regard to its power. A comparable study has been done by Solmaz and Karabulut [50] who study the influence of kinematics on performance of a beta-type Stirling engine. It is interesting to know if a crank-connecting rod system is the most adapted solution and if the optimal configuration depends on the working gas. Therefore, the motor presented in Section 2 is used as baseline. As the volumes of the hot side and the cold side at any moment of the cycle are defined by the dimension (Table 1) as well as the kinematics, it is very helpful to have a modular approach to describe the motor volumes in function of dimensions and kinematics, (Fig. 11). Here, the initial kinematic function has been replaced by a matrix that will be changed by the optimization. This matrix contains discretized values of displacement with a precision of 6° of crankshaft angle. The particles evolve thus in 123 dimensions: 61 for the kinematic of each piston and 1 for their phase shift.

In order to respect the dimensional characteristics of the motor, each kinematic point has to be between 0 and the stroke, the phase shift has to be between 0 and 360°. The evolution of the profile is constrained in order to be cyclic with a maximum and a minimum position. Furthermore, the maximum distance between two matrix points is constrained in order to limit the accelerations of the pistons.

The kinematics of the motor are optimized for a rotational speed of 300 rpm and working gases air and helium. Other parameters are considered as constant with an absolute filling pressure of 11 bar and a hot source temperature of 700 °C.

5.3. Application using air

The results of optimization are presented in Fig. 12. They show the same general kinematics as the initial crank-connecting rod system, but three basic differences can be identified: Firstly, the pistons motions are not continuous. They present a halt at the minimum and maximum position. Secondly, the movement of the motor piston is less symmetric than the behavior of the displacer piston. It shows a steeper ascent than decent. Finally, this leads to the fact that the phase shift throughout a cycle varies between 90° at the beginning of the cycle to 100° at the maximum position of each piston.

The modification of the kinematic influences directly the volume curves, (Fig. 13). The volume in the hot zone depends only on the position of the displacer piston and has thus the same shape as the kinematic. The volume in the cold zone depends on both pistons. The main influence of the new kinematic takes place at the beginning of the compression and at the beginning of the expansion. The beginning of the compression is defined by the lack of gas

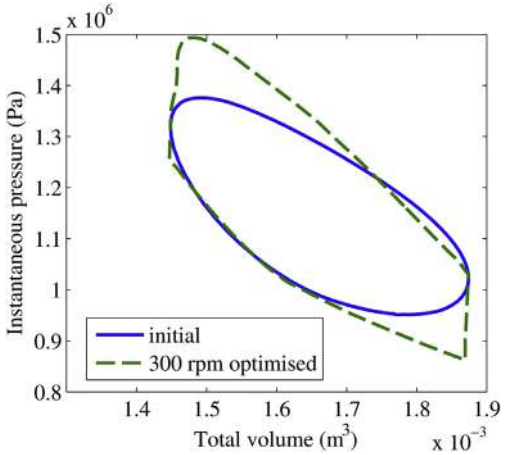

Fig. 14. Optimized PV diagram: air, 10 bar, 300 rpm, 700 °C.

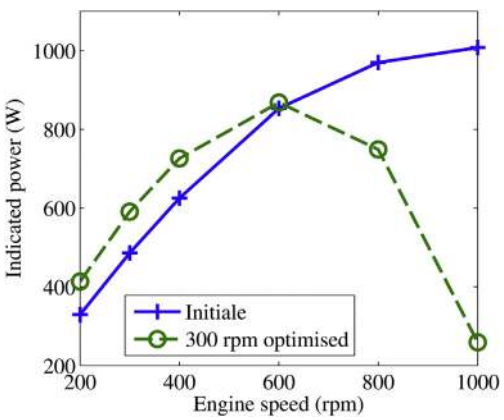

Fig. 15. Influence of optimized kinematics air, 10 bar, 700 °C.

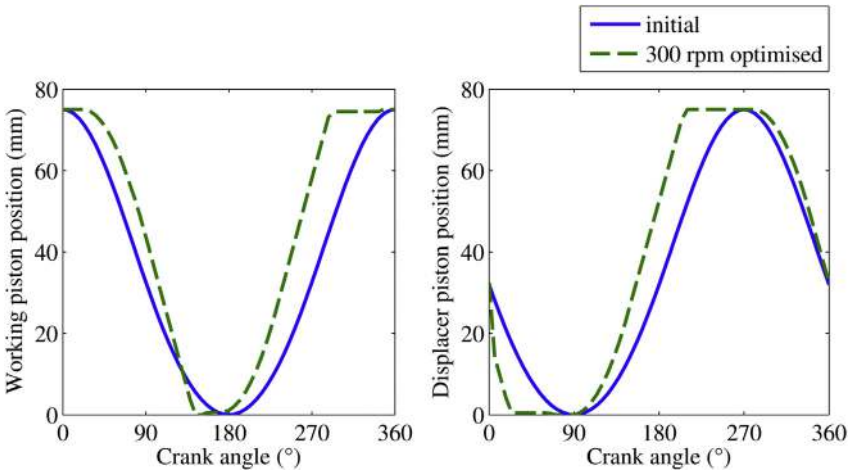

Fig. 16. Optimized piston kinematics: helium, 10 bar, 300 rpm, 700 °C.

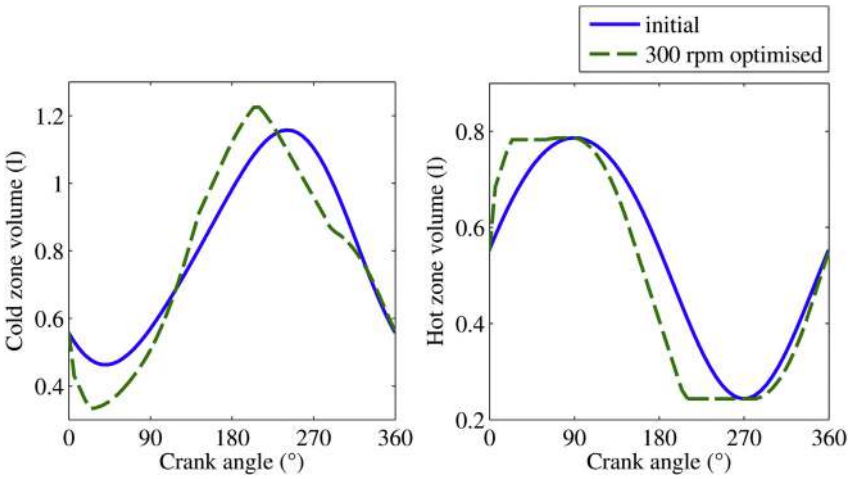

Fig. 17. Optimized volumes: helium, 10 bar, 300 rpm, 700 °C.

transfer, the biggest fraction of the gas stays in the cold zone. Likewise, at the beginning of the expansion the biggest fraction of the gas stays in the hot zone. The decanting between hot and cold zone is thus more rapid, which is represented in the PV diagram. It can be seen that the heating and cooling processes get closer to the isochoric process, and the cycle comes closer to the Carnot cycle and demonstrates thus an increase in power, (Fig. 14).

Finally, the influence of the new kinematics over the entire speed range is shown in (Fig. 15). It can be seen that the optimized kinematics lead to a power increase at low rotation speeds, but show a lower maximum power than the initial configuration. Moreover, this maximum power occurs at lower rotational speeds, (our optimization being processed for 300 rpm). This observation underlines the fact, that the configuration of a Stirling engine depends strongly on the working condition and that a configuration, that is well adapted to one working point can be suboptimal for another working point.

5.4. Application using helium

The kinematics of the motor using helium is also optimized for a rotational speed of 300 rpm with an absolute pressure of 11 bar and a hot source temperature of 700 °C. The results of optimization are presented in Fig. 16, the same conclusions as for air can be adopted for helium as working gas, namely: the pistons show a halt at the minimum and maximum position; the movement of the motor piston is less symmetric than the movement of the displacer piston. And that the phase shift throughout a cycle varies between 90° at the beginning to 100° at the maximum position of each piston.

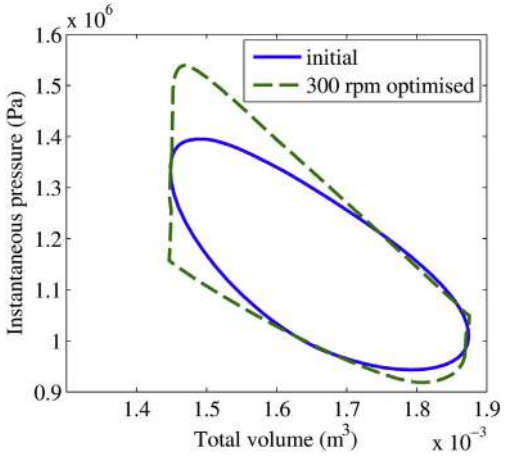

Fig. 18. Optimized PV diagram: helium, 10 bar, 300 rpm, 700 °C.

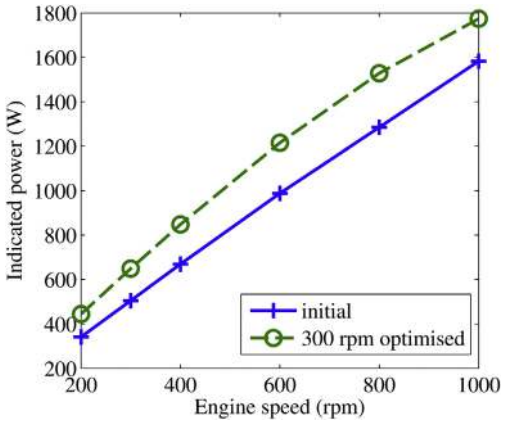

Fig. 19. Influence of optimized kinematics helium, 10 bar.

The modification of the kinematic influences directly the volume curves, (Fig. 17), thus leading to a bigger variation of the cold zone volume. The decanting between hot and cold zone is thus more rapid, represented by a PV diagram which is closer to the ideal representation and demonstrates the increase in power that can be obtained, (Fig. 18). Furthermore, Fig. 18 seems to show a larger increment of area when passing from initial to optimized kinematic than in the case of air (Fig. 14). This assumption is confirmed by comparison of power gain for helium and air at 300 rpm (Figs. 15 and 19). Nevertheless, comparison of Figs. 14 and 18 also reveals a difference between the two gases. At 300 rpm, in the case of air, optimization leads to an optimized PV diagram that approaches the Carnot cycle, for both minimum and maximum volume of the cycle, but with helium the optimized PV diagram does hardly vary from the initial PV diagram for maximum volume of the cycle.

Finally, the influence of the new kinematics over the entire speed range is shown in Fig. 19. It can be seen that the optimized kinematics lead to a nearly constant power increase in the evaluated speed range. Former observations (Fig. 5) have already shown that the maximum power is expected for higher engine speeds. Furthermore, it has been shown in Fig. 15 that the optimization of kinematics for a Stirling engine working on air, increased the power at low rotational speeds, but also pushed the maximum power available to lower rotational speeds and decreases the maximum power that can be achieved.

It is plausible that this phenomenon is also taking place using helium as working gas, and that the speed range was only too low to observe it. This is why the speed range has been broaden for the simulation and Fig. 20 confirms that a maximum engine power with the optimized kinematics is expected at 1500 rpm.

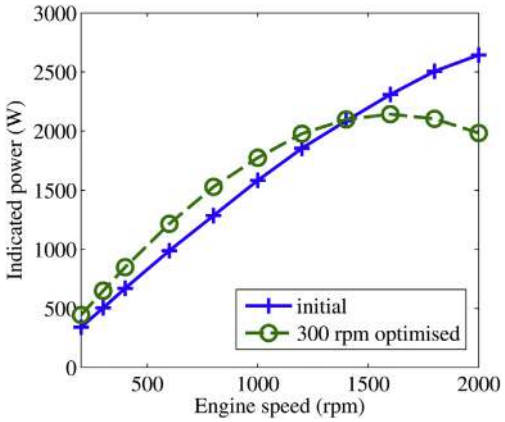

Fig. 20. Influence of optimized kinematics helium, 10 bar, larger range.

In conclusion it can be said that the optimization led to improved power output for the given system parameters, but analysis show that the optimized kinematics are quite close to a crankshaft converting rod system independently of the working gas. Moreover, the power increase at the given working point leads to a lower maximum power at lower rotational speeds.

6. Conclusion

In the study presented in this article, a tool to pre-dimension the characteristics of a Stirling engine devoted to a given application has been developed. Therefore, this work presents the experimental validation of a numerical zero dimensional, three zones model of the engine with time dependent heat and mass exchanges. A modular modeling approach is chosen in order to adapt Stirling engine dimensions and kinematics easily and without the need to change the model. Pressure drops are included to the model using experimental measurements for air. It is shown that the transposition of air pressure drops to helium has negative influence to model accuracy, but the model stays viable enough to bring admissible results.

The simulation results are validated using a 1 kW Stirling engine with different working gases (air and helium), gas pressure (between 1 bar absolute for air and 2 bar absolute for helium up to 11 bar absolute for both), hot source temperature (between 200°C and 700°C) and rotational speed (between 200 rpm and 1000 rpm).

The validation between numerical and experimental results shows good agreement with regard to the effective power for a variation of speed, filling pressure and hot source temperature. A special emphasis is put on the experimental validation of the model with regard to the two different working gases air and helium.

The influence of the working gas on the effective power can thus be explained. The experiments underline that air shows a higher power potential at low speed and helium shows a better potential at high working speeds. So according to the designated working point the most adapted working gas should be chosen.

Finally, the validated model has been associated to a particle swarm optimization algorithm to develop a Stirling engine design optimization tool. This tool is tested for the optimization of the kinematics of the engine for a given working condition (rotational speed of 300 rpm, pressure of 10 bar, hot source temperature of 700°C, with air and helium). Results show that the optimum solution is close to a crankshaft connecting rod system solution. An improvement of power of 22% can be obtained for both working gases. The effective power increase that can be obtained for this low speed working point, leads to a limited maximum power. Whereas for helium as working gas the gain in power that can be realized by the optimized kinematics is maintained over the tested range of speeds.

In the future, it would be interesting to refine the description of pressure drops in function of the working gas used, to validate the model for different Stirling engines with different dimensions and power ranges and to improve the study on different working gases. Moreover, it could be interesting to enlarge the model, validation and optimization to cryogenic Stirling systems.

Acknowledgment

Authors would like to thank Burgundy region council for continuous support of ID-MOTION lab.

References

[1] Podesser E. Electricity production in rural villages with a biomass Stirling engine. Renew Energy 1999;16(1–4):1049–52.
[2] Sternlicht B. Waste energy recovery: an excellent investment opportunity. Energy Convers Manage 1982;22:361–73.
[3] Ahmadi MH, Mohammadi AH, Dehghani S, Barranco-Jimenez MA. Multi-objective thermodynamic-based optimization of output power of solar dish-Striling engine by implementing an evolutionary algorithm. Energy Convers Manage 2013;75:438–45.
[4] Ahmadi MH, Sayyaadi H, Dehghani S, Hosseinzade H. Designing a solar powered Stirling heat engine based on multiple criteria: maximized thermal efficiency and power. Energy Convers Manage NOV 2013;75:282–91.
[5] Petrescu S, Petre C, Costea M. A methodology of computation, design and optimization of solar Stirling power plant using hydrogen/oxygen fuel cells. Energy February 2010;35(2):729–39. conference: 21st International Conference on Efficiency, Cost, Optimization, Simulation and Environmental Impact of Energy Systems Location: Cracow, POLAND Date: JUN 24–27, 2008.
[6] Blank DA, Wu C. Power optimization of an extraterrestrial, solar-radiant Stirling heat engine. Energy June 1995;20(6):523–30.
[7] Stirling R. UK patent n 4081. 1816.
[8] Karabulut H, Cinar C, Öztürk E, Yücesu H. Torque and power characteristics of a helium charged Stirling engine with a lever controlled displacer driving mechanism. Renew Energy 2010;35(1):138–43.
[9] Dong H, Zhao L, Zhang S e a. Using cryogenic exergy of liquefied natural gas for electricity production with the Stirling cycle. Energy December 2015;63: 10–8.
[10] Cullen B, McGovern J. Energy system feasibility study of an otto cycle/Stirling cycle hybrid automotive engine. Energy 2010;35:1017–23.
[11] Kongtragool B, Wongwises S. A review of solar-powered Stirling engines and low temperature differential Stirling engines. Renew Sustain Energy Rev 2003;7:131–54.
[12] Abbas M, Said N, Boumeddane B. Thermal analysis of Stirling engine solar driven. Rev des Energies Renouvelables 2008;11(4):503–14.
[13] Blank DA. Universal power optimized work for reciprocating internally reversible Stirling-like heat engine cycles with regeneration and linear external heat transfer. J Appl Phys 1998;84(5):2385–92.
[14] Costea M, Feidt M. The effect of the overall heat transfer coefficient variation on the optimal distribution of the heat transfer surface conductance or area in a Stirling engine. Energy Convers Manage 1998;39(16–18):1753–61.
[15] Kaushik SC, Kumar S. Finite time thermodynamic analysis of endoreversible Stirling heat engine with regenerative losses. Energy October 2000;25(10): 989–1003.
[16] Kongtragool B, Wongwises S. Thermodynamic analysis of a Stirling engine including dead volumes of hot space, cold space and regenerator. Renew Energy 2006;31:345–59.
[17] Puech P, Tishkova V. Thermodynamic analysis of a Stirling engine including regenerator dead volume. Renew Energy 2011;36:872–8.
[18] Schmidt G. Theorie der lehmannchen calorischen mashine. Zeit Des Vereines deutsch Ing 1871;15:97–112.
[19] Tamura T, Kitagawa S, Fukuyama Y. Optimal operational planning for cogeneration system using particle swarm optimization. In: Swarm Intelligence Symposium, 2003. SIS'03. Proceedings of the 2003 IEEE. IEEE; April 2003. p. 138–43.
[20] Urieli I, Kushnir M. The ideal adiabatic cycle – 1a rational basis for Stirling engine analysis. In: IECEC'82; Proceedings of the Seventeenth Intersociety Energy Conversion Engineering Conference, vol. 4; August 1982. p. 1662–8. Los Angeles, USA.
[21] Ahmadi MH, Hosseinzade H, Sayyaadi H, Mohammadi AH, Kimiaghalam F. Application of the multi-objective optimization method for designing a powered Stirling heat engine: design with maximized power, thermal efficiency and minimized pressure loss. Renew Energy Dec 2013;60: 313–22.
[22] Toghyani S, Kasaeian A, Ahmadi MH. Multi-objective optimization of Stirling engine using non-ideal adiabatic method. Energy Convers Manage 2014;80(0):54–62.
[23] Ahmadi MH, Mohammadi AH, Pourkiaei SM. Optimisation of the thermodynamic performande of the Stirling engine. Int J Ambient Energy 2014.
[24] Wouagfack PAN, Réné T. Finite-time thermodynamics of optimization of absorption refrigeration systems: a review. Renew Sustain Energy Rev 2013;21: 524–36.
[25] Kantor J, Mousaw P. A class of bilinear model for the optimization of energy conversion networks. Chem Eng Sci 2012;67:131–8.
[26] Ladas H. Finite-time view of the Stirling engine. Energy August 1994;19(8): 837–43.
[27] Costa SC, Barrutia H, Esnaola JA, Tutar M. Numerical study of the pressure drop phenomena in wound woven wire matrix of a Stirling regenerator. Energy Convers Manage 2013;67:57–65.
[28] Timoumi Y, Tlili I, Ben Nasrallah S. Performance optimization of Stirling engines. Renew Energy 2008;33:2134–44.
[29] Özgören YO, Çetinkaya S, Saridemir S, Çiçek A, Kara F. Predictive modeling of performance of a helium charged Stirling engine using an artificial neural network. Energy Convers Manage 2013;67:357–68.
[30] Chen C-H, Yang H-S. Optimization of rhombic drive mechanism used in beta-type Stirling engine based on dimensionless analysis. Energy January 2014;64:970–8.
[31] Creyx M, Delacourt C e a, Morin E. Energetic optimization of the performances of a hot air engine for micro-CHP systems working with a joule or an Ericsson cycle. Energy January 2013;49:229–39.
[32] Campos MC, Vargas JC, Ordonez JC. Thermodynamic optimization of a Stirling engine. Energy August 2012;44(1):902–10.
[33] ve-ingenieure. Datasheet st05-g Striling engine. September 2014 [Online]. Available from: http://www.ve-ingenieure.de/projekt_st05g_cnc_engl.html.
[34] Chen W-L, Wong K-L, Chen H-E. An experimental study of the performance of the moving regenerator for a gamma-type twin power piston Stirling engine. Energy Convers Manage 2013;77:118–28.
[35] Bert J, Chrenko D, Sophy T, Le Moyne L, Sirot F. Zero dimensional finite-time thermodynamic, three zones numerical model of a generic Stirling and its experimental validation. Renew Energy November 2012;47:167–74.
[36] Andersen SK, Carlsen H, Thomsen PG. Preliminary results from simulations of temperature oscillations in Stirling engine regenerator matrices. Energy 2006;31:1371–83.
[37] Cheng C-H, Yu Y-J. Numerical model for predicting thermodynamic cycle and thermal efficiency of a beta-type Stirling engine with rhombic-drive mechanism. Renew Energy 2010;35:2590–601.
[38] Shampine LF, Hosea ME. The Matlab ODE suite. SIAM J Sci Comput 1997;18: 1–22.
[39] Shampine LF, Reichelt MW, Kierzenka J. Solving index-1 DAES in MATLAB and Simulink. SIAM Rev 1999;41:538–52.
[40] Formosa F, Frechette LG. Scaling laws for free piston Stirling engine design: benefits and challenges of miniaturization. Energy August 2013;57:796–808.
[41] Seghir-Ouali S, Saurya D, Harmand S, Phillipart O, Laloy D. Convective heat transfer inside a rotating cylinder with an axial air flow. Int J Therm Sci 2006;46:1166–78.
[42] Colburn AP. A method of correlating forced convection heat transfer data and a comparison with fluid friction. Trans AIChE 1933;29:174–210.
[43] Guibert P. Moteur à allumage commandé. Techniques de l'ingénieur 2005:BM 2 511.
[44] Yun KT, Cho H, Luck R, Mago PJ. Modeling of reciprocating internal combustion engines for power generation and heat recovery. Appl Energy 2012;(0).
[45] Incropera FP, De Witt DP. Fundamentals of heat and mass transfer. 4th ed. New York: Wiley; 2000.
[46] Burcat A, Ruscic B. Third millennium ideal gas and condensed phase thermochemical database for combustion with updates from active thermochemical tables. ARGONNE National Laboratory, TACHNION Isreal Institute of Technology; September 2005.
[47] Karabulut H, Yücesu HS, Cinar C, Aksoy F. An experimental study on the development of a beta-type Stirling engine for low and moderate temperature heat sources. Appl Energy 2009;86(1):68–73.
[48] Elbeltagi E, Hegazy T, Grierson D. Comparison among five evolutionary-based optimization algorithms. Adv Eng Inform 2005;19:43–53.
[49] Eberhart R, Kennedy J. A new optimizer using particle swarm theory. In: Micro machine and Human science, 1995. MHS'95., Proceedings of the Sixth International Symposium on. IEEE; Octobre 1995. p. 39–43.
[50] Solmaz H, Karabulut H. Performance comparison of a novel configuration of beta-type Stirling engines with rombic drive engine. Energy Convers Manage 2014;78:627–33.